Acoustically Activated Nozzle for Microdroplet Generation and Dispensing

Qiu Yin,[1] Xiuyuan Li,[1] Zhichao Ma,[2,*] and Wenming Zhang[1,†]

[1] *State Key Laboratory of Mechanical System and Vibration, Shanghai Jiao Tong University, Shanghai 200240, China*

[2] *Institute of Medical Robotics, School of Biomedical Engineering, Shanghai Jiao Tong University, No. 800 Dongchuan Road, Shanghai 200240, China*

(Received 31 May 2023; revised 25 June 2023; accepted 3 August 2023; published 25 August 2023)

Droplet-based microfluidic has emerged as a versatile tool for widespread applications, such as biochemical analysis and synthesis, for which the generation and manipulation of the microdroplets are fundamental. Acoustic based droplet control has shown advantages of good biocompatibility and widescale tunability. Here, we demonstrate an acoustic controlled nozzle that is integrated with both generation and directed dispensing of microdroplets. The system can generate monodisperse microdroplets with tunable sizes (50–641 μm) at a highest throughput of 2000 droplets per second. Besides, by tuning the acoustic frequency, the droplets can be steered to different directions after their formation, realizing on-demand dispensing of the microdroplets. The controlled microdroplet generation and dispensing are both attributed to the acoustic streaming effect induced by the nozzle vibration. Two basic mechanisms for the droplet control were studied: (1) the correlation between the droplet size and the acoustic actuation time, (2) the dependence of the droplet dispensing direction on the acoustic frequency. This work paves the way towards programmable control over acoustic generation and dispensing of microdroplets, which has great potential in the applications of bio-chemical analysis and synthesis.

DOI: 10.1103/PhysRevApplied.20.024067

I. INTRODUCTION

Droplet microfluidics focus on generation and manipulation of droplets in the femto- to nanoliter volume range [1,2]. The microdroplets have high surface area to volume ratios, thus providing faster heat and mass transfer rate compared to the macroscale chemical reactors. And they can be massively produced in portable devices and then individually controlled for mixing, heating, and sensing. Thus, droplet microfluidics have emerged as a fundamental technology for versatile biochemical analysis [3]. For example, microdroplet-based digital polymerase chain reaction (DPCR) [4], digital loop-mediated isothermal amplification (DLAMP) [5], and single-cell analysis [6]. Moreover, the generation and manipulation of microdroplets also benefit drug delivery [7], tissue engineering [8] and, single-cell cultivation [9]. In recent decades, there have been considerable research efforts devoted to studying microdroplet generation and manipulation, which bring up the advances in the above fields [10,11].

In terms of droplet generation, the microfluid devices can control the microdroplet size and generation rate by varying the flow rates [12], hydraulic pressure [13,14], or channel geometry (e.g., T junction [15,16], flow focusing [17,18], co-flow [19]). In addition, to enhance the controllability over droplet generation, energy inputs other than basic pumping can be added to modulate the balance between shear stress and the surface tension during droplet formation, including electrical [20], magnetic [21], optical [22], thermal [23], and acoustic actuations [24]. These external field inputs not only provide active control over droplet size [25] but also enable on-demand droplet generation [26], which benefit single-cell analysis and digital PCR [27,28].

Apart from droplet generation, manipulation of the discrete droplets (e.g., dispensing [29], separation [30], and delivery [31]) also attract great research interests where the external fields bring up the capability of active control [32]. For example, dielectrophoresis actuated microdroplet movement can direct them to the target outlets in a microfluidic system, which can be controlled by a fluorescence detection system and compose the so-called fluorescence-activated droplet sorter [29,30,33]. In a similar manner, acoustic wave can also direct the droplet flow and then sort the encapsulated cell within the droplets [34,35]. To actively sort the droplets with different inclusion amount, Huang *et al*. develop a single-step droplet generation and sorting system based on the hydrodynamic force at a vibrating interface [36].

*zhichaoma@sjtu.edu.cn
†wenmingz@sjtu.edu.cn

Among the various external field droplet control, acoustic methods show the advantages of good compatibility, fast response, and widescale tunability, and thus have innovated the strategies of droplet microfluidics [37]. Moreover, the ultrasound microdevices can be easily integrated with microfluid environment and have low cost and save the effort for magnetic or electrical labeling. For example, Riefler *et al*. showed a microdroplet generation system based on the fluid interface vibration. When the fluid at the interface nozzle tip resonates at a certain amplitude, it overcomes the surface tension to eject microdroplets [38]. Besides, acoustic waves can activate droplet generation based on acoustic-pressure-induced jetting [39,40]. The generation rate is around 20 per second [41]. Foresti *et al*. developed an acoustophoretic three-dimensional (3D) printing method, the ejection rate increases up to values of 1000 Hz [24]. Recently, He *et al*. proposed a method based on vibrating sharp-tip capillary, which can produce droplets with high throughout up to 5000 Hz. The acoustic vibration at the sharp-tip capillary generates acoustic streaming that extrudes the discrete phase to form microdroplets. The size of the microdroplets is controllable based on the acoustic modulation [42]. Based on a similar mechanism, the same group demonstrated the application of the droplet generation system for digital bacteria enumeration and antibiotic susceptibility testing [43]. Besides droplet generation, acoustic methods can also be used in droplet manipulation, including size control [44,45], separation [46,47]. The integration of controllable droplet generation and manipulation is preferred in biomedical analyses, such as fluorescence activated droplet sorting (FADS) [29], droplet-based drug release [36], and organism assembly [48]. For example, Li *et al*. demonstrated a strategy of droplet generation and manipulation based on interfacial vibration at the nozzle tip. High-intensity vibration overcame the surface tension to generate droplets, while low-intensity vibration generated a hydrodynamic field that moved the discrete droplets [49]. These works show that acoustic methods are promising for droplet generation and manipulation. However, high-throughput production of droplets and dispensing are conducted in a separate manner, which is not fulfilling the requirements in the applications of biochemical analysis. There still lacks an acoustic method for integrating high-throughput droplet generation and dispensing.

In this paper, we demonstrate an acoustic actuated droplet microfluidic nozzle that integrates generating and dispensing of microdroplets. The modulated acoustic waves transmit through the nozzle and induce acoustic streaming flows that extrude the fluid at the nozzle tip and form microdroplets. The microdroplets' production rate can reach 2000 droplets per second. The correspondence between microdroplet size and the acoustic actuation time is studied, which shows a positive correlation between them. The formed microdroplets have a wide size range (50–641 μm) that can be actively controlled based on acoustic actuation time. Interestingly, we find that the acoustic streaming profile at the nozzle tip is determined by acoustic frequency. Thus, the microdroplets can then be steered and dispensed to on-demand zones based on the acoustic streaming flow direction by tuning the acoustic frequency. Numerical simulation verifies the acoustic streaming profiles change based on different acoustic frequency. These studies pave the way for an integrated acoustofluidic device for droplet generation and dispensing. And the acoustic device provides a good biocompatibility, simple setup, and portable size. Considering the wide applications of droplet generation and dispensing in biochemical analysis [1,3,12] and the advantages of acoustic control [32], the present system has the potential to improve the high-throughput analyzing equipment, such as cytometer and digital PCR device.

II. MATERIAL AND METHODS

A. Device fabrication

To fabricate the droplet generation and dispensing system, we attached a PZT transducer to one side of a metal plate at first, and then a pulled-tip glass capillary was glued to the center of the PZT transducer with the tip extending about 1.5 cm beyond the glass slide. The length of the pulled tapered part is 5 mm and the outer diameter (OD) of the tips of the prepulled glass capillaries is about 20 μm. The upper end of the glass capillary is connected to the polyethylene tube. As shown in the simulation results in Tables S3 and S4 within the Supplemental Material [52], both the distance between the nozzle and the piezoelectric plate and the capillary tube diameter influence the acoustic resonant frequency. Moreover, the depth of the nozzle tip immersed in oil is kept constant as 5 mm during the experiment. The variation of this depth may influence the resonance magnitude among different devices. Thus, it is useful to keep these parameters constant among the experiments or the devices. We first filled the tube with water or alginate (Sigma W201502) solution using a syringe, then inserted one end of the polyethylene tube into a container filled with water. In addition, we prepared the oil phase by mixing mineral oil with EM 90 (3%), filled it in a droplet tank made of glass, and inserted the lower end of the glass tube into the oil phase. During the working process, the PZT transducer was driven by a signal generator (AFG3022C, Tektronix, USA) and a voltage amplifier (ATA-1372A, Aigtek, China).

B. Characterization of droplet generation and dispensing

The droplet formation and dispensing process were recorded using a high-speed camera (5KF20M). The optical images of the droplet were taken by digital microscope

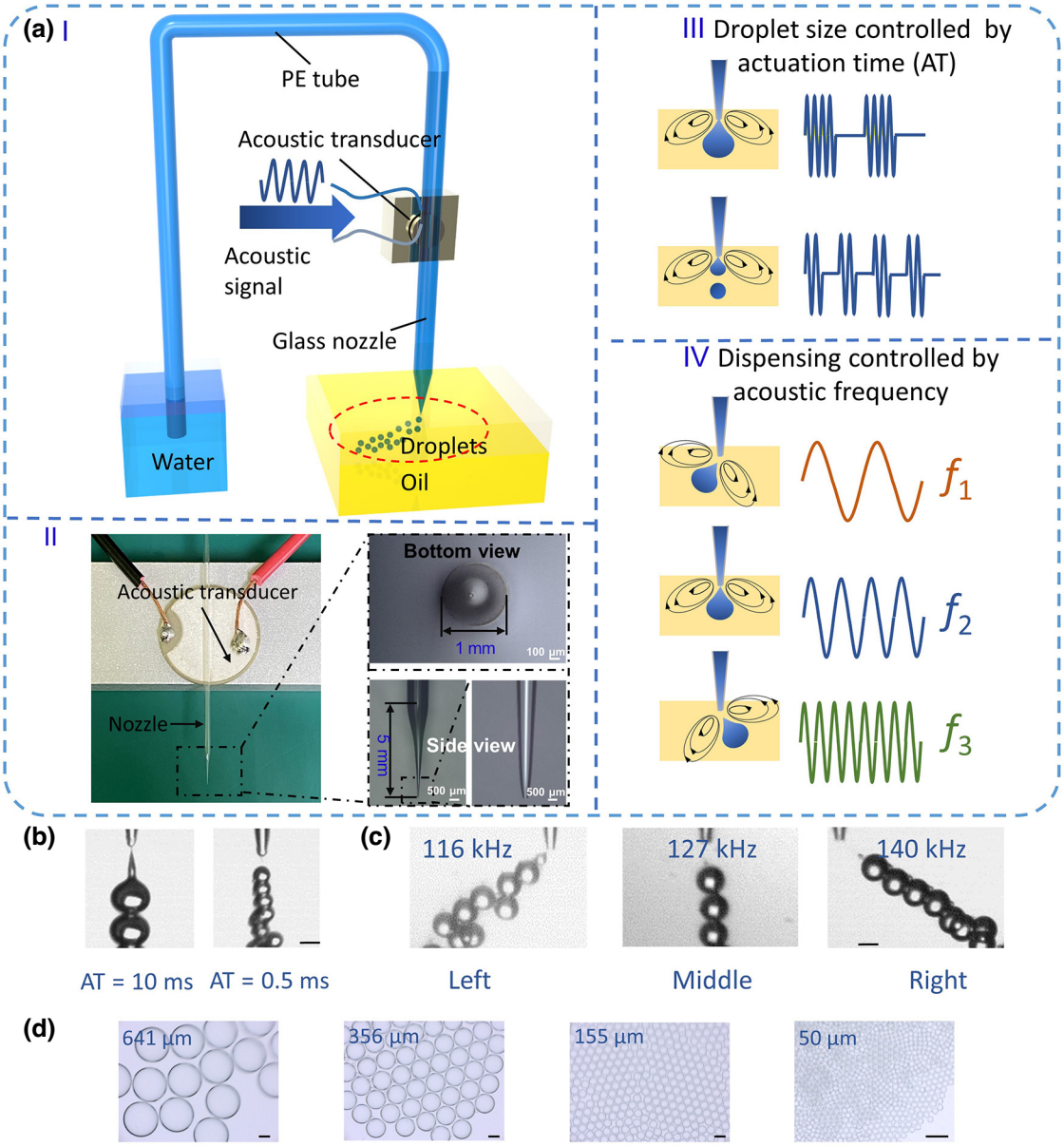

FIG. 1. The acoustic activated nozzle for both microdroplet generation and dispensing. (a) The schematic of the operating principle. (I), (II) The system consists of a nozzle and the acoustic transducer attached to it. When the nozzle is filled with water and immersed in the oil and the water-oil interface is balanced right at the nozzle tip. While the PZT transducer is applied with a modulated alternative current signal, the transducer generates acoustic waves, which transmit to the nozzle tip, then the water in the nozzle will extrude and form microdroplets. (III) The microdroplet size is positively correlated to the acoustic actuation time (AT). (IV) The droplets can be dispensed at different directions while the acoustic frequency changes. (b) The microdroplet size decreases as the acoustic AT decreases from 10 to 0.5 ms. Scale bar: 100 μm. (c) At the acoustic frequencies of 116, 127, and 140 kHz, the droplets are directed to the left, middle, and right of the nozzle tip, respectively. Scale bar: 100 μm. (d) Combining the controls of both droplet size and directions, the acoustic activated nozzle can regulate the microdroplet on-demand size and dispensing direction. Scale bar: 200 μm.

(Keyence VHX-7000). And the diameters of droplets were obtained by analyzing the images using ImageJ software.

C. Numerical simulation

In order to explore the motion and dynamic characteristics of the system, the modal analysis of the device is conducted by the ABAQUS finite-element package with a linear perturbation-frequency module. Here, the model consists of the PZT actuator, the glue layer and the capillary tube. One side of the PZT actuator is applied to a fixed boundary condition. The glue part bonds the capillary tube and the PZT actuator together. It covers part of the capillary tube, and its thickness is 0.1 mm, the geometry

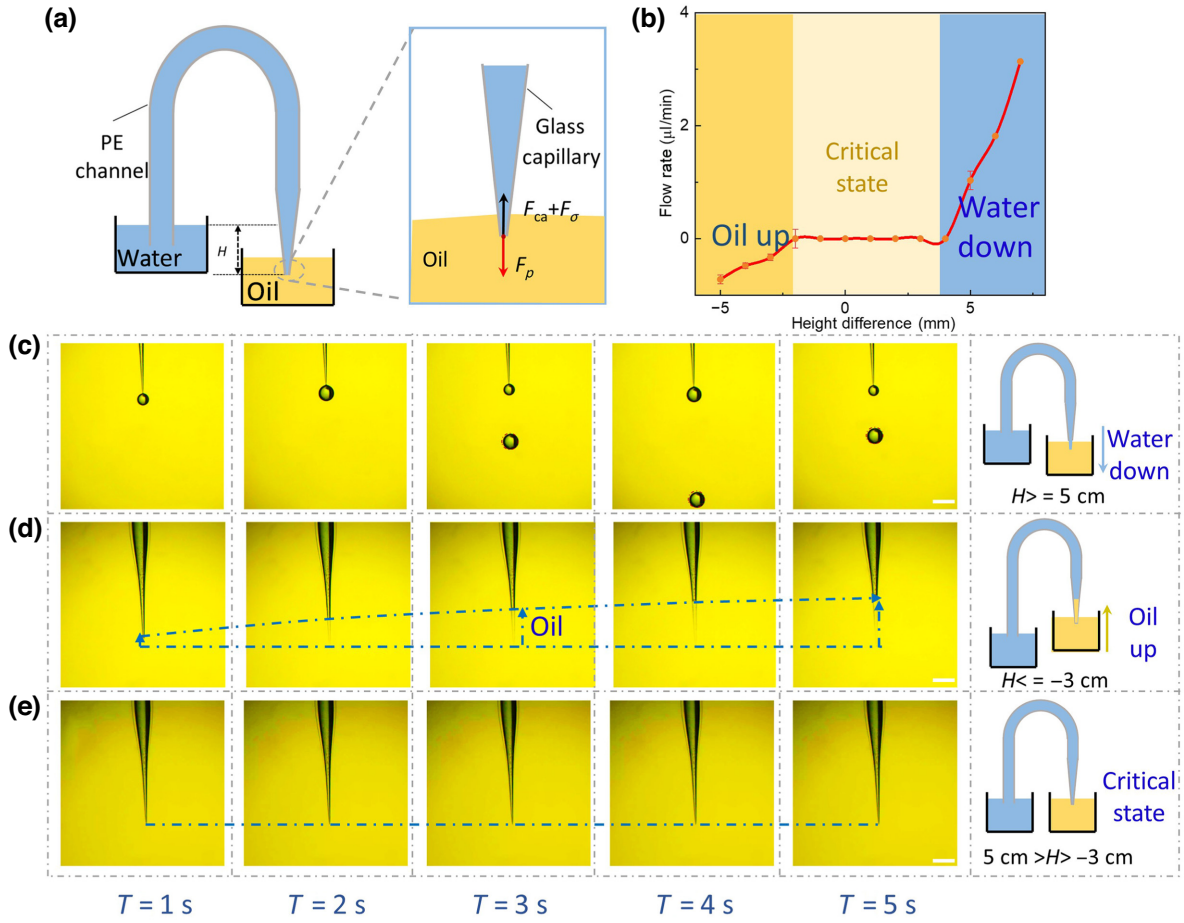

FIG. 2. The hydraulic pressure regulation setup for controlling the water-oil interface. (a) The hydraulic pressure is regulated based on the height difference between the water-air interface and the oil-air interface. (b) The flow rate of the nozzle filament (water) increases as the height difference increases. (c)–(e) By tuning the height difference, the position of the water-oil interface can be controlled. (e) At the critical state, the water-oil interface stabilizes at the nozzle tip, where acoustic waves can activate the droplet generation. Scale bar: 1 mm.

of the capillary tube is obtained via Keyence VHX-7000 microscope measurements. The distance between nozzle end and PZT is 15 mm. The vibration modes and nature frequencies of the whole structure and capillary tip can both be obtained.

Furthermore, to explore the mechanism of microdroplet generation and dispensing, the numerical modeling of acoustic streaming field was conducted with the finite-element method (FEM) software COMSOL Multiphysics, similar to a previously published method [50]. To simplify the calculation, we used a two-dimensional model. And the numerical simulation process consists of three steps. First, the solid mechanics and pressure acoustics module in the frequency domain was employed to solve the acoustic field produced by a piezoelectric plate and propagating along the nozzle. Then, the thermoviscous acoustics module in the frequency domain was used to obtain the first-order acoustic velocity fields, where the nozzle vibration calculated from the last module was substituted as the initial boundary conditions of the oil phase. Finally, the body force calculated from the thermoviscous acoustics module was substituted to the laminar flow module to calculate the acoustic streaming profile (more detail of the numerical simulation can be seen within the Supplemental Material [52]).

III. RESULTS AND DISCUSSION

The operation principle and the schematic of the setup is shown in Fig. 1(a) I and II. The system consists of a capillary nozzle, a PZT transducer, a hydraulic pressure regulation reservoir filled with water, and a collection reservoir filled with oil. While the PZT transducer is applied with an alternative current signal, the transducer generates acoustic waves, which transmit through the capillary to the nozzle tip, the liquid in the nozzle will be pumped out. When the modulated acoustic energy

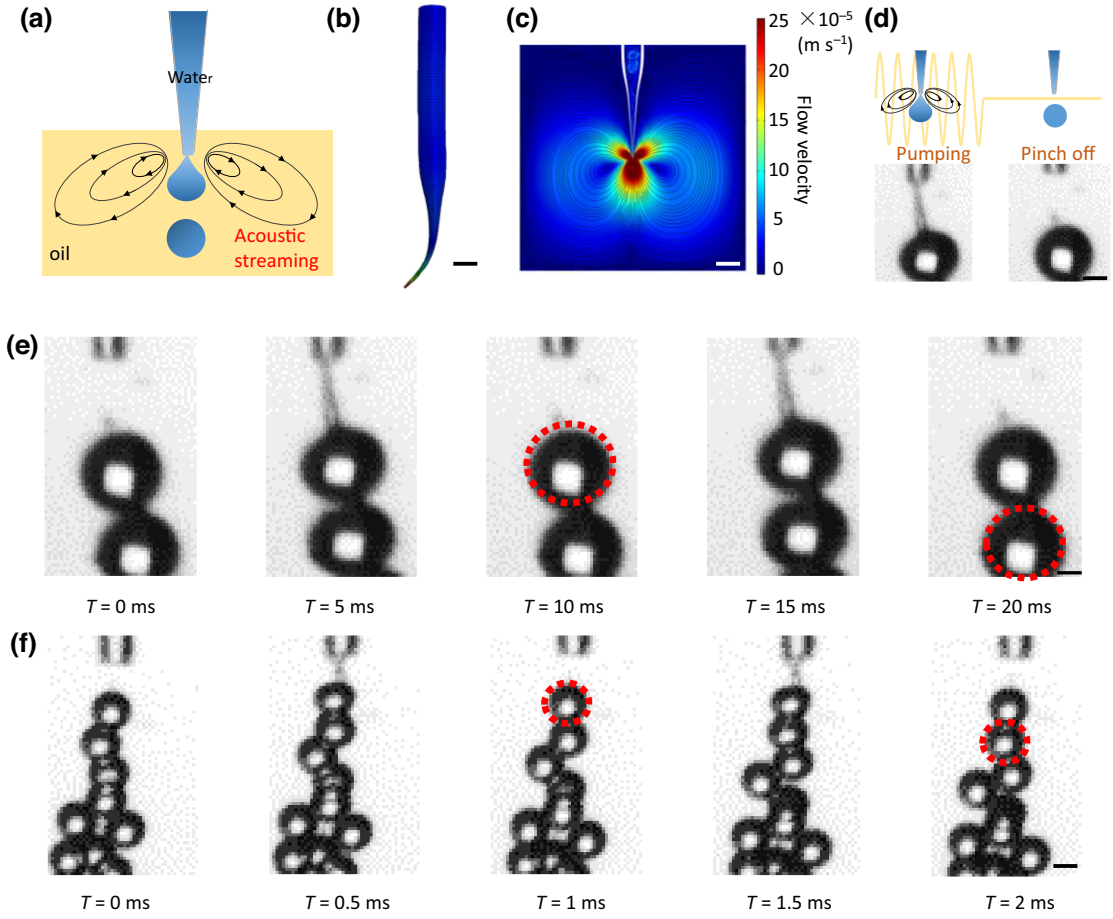

FIG. 3. Acoustic controlled microdroplet generation. (a) While the acoustic is turned on, the induced acoustic streaming effect extrude the water from the nozzle tip. (b) Numerical simulation shows the nozzle vibration actuated by the transducer. Scale bar: 1 mm. (c) Numerical simulation presents the acoustic streaming effect from the nozzle vibration. Scale bar: 1 mm. (d) The process of droplet generating includes the water extrusion and pinch off while the acoustic is turned on and off, respectively. Scale bar: 50 μm. (e),(f) The generated microdroplet size can be controlled by tuning of the actuation time [(e) AT = 5 ms; (f) AT = 0.5 ms]. Scale bar: 50 μm.

transferred to liquid phase, the intermitted acoustic streaming occurred [51]. While the vibration is turned on, the water is pumped out from the nozzle. And while the vibration is turned off, the extruded water will break into a droplet due to the Laplace pressure. Therefore, the actuation time of acoustic wave determines the amount of water coming out from the nozzle, which is the size of the formed droplets [Fig. 1(a) III]. Interestingly, we find that the droplets translate to different directions while different acoustic frequencies are applied on the capillary. As shown in Fig. 1(a) IV, when the acoustic frequency changed, the nozzle vibrates at different modes, thus inducing different acoustic streaming profiles. The streaming flow will then exert a draft force on the generated droplets at the nozzle tip then direct them to the corresponding directions. As shown in Fig. 1(b) of experimental tests, by differing the actuation time of 0.5 and 10 ms, the generated droplet has a corresponding diameter of 79 and 208 μm, respectively. We also find three acoustic frequencies at which the generated microdroplets are directed to the left, middle, and right of the nozzle, respectively [Fig. 1(c)]. In combination of the droplet generation and steering, we demonstrate generating droplets with on-demand sizes and steer them immediately to different collection zones [Fig. 1(d)].

In order to adjust the water-oil interface located at the nozzle tip, we used two reservoirs, respectively, containing water and oil and regulated the water-oil interface by tuning their height difference. The schematic is shown in Fig. 2(a). The water-oil interface was governed by the gravity (G) and hydraulic pressure (F_p) produced by the height difference between water-air and oil-air interfaces, capillary force (F_{ca}) produced by the capillary interface, and the interfacial force (F_σ). Thus, while the other properties keep constant, the positions of the water-oil interface has a correspondence to the hydraulic pressure, which is the height difference between water-air and oil-air

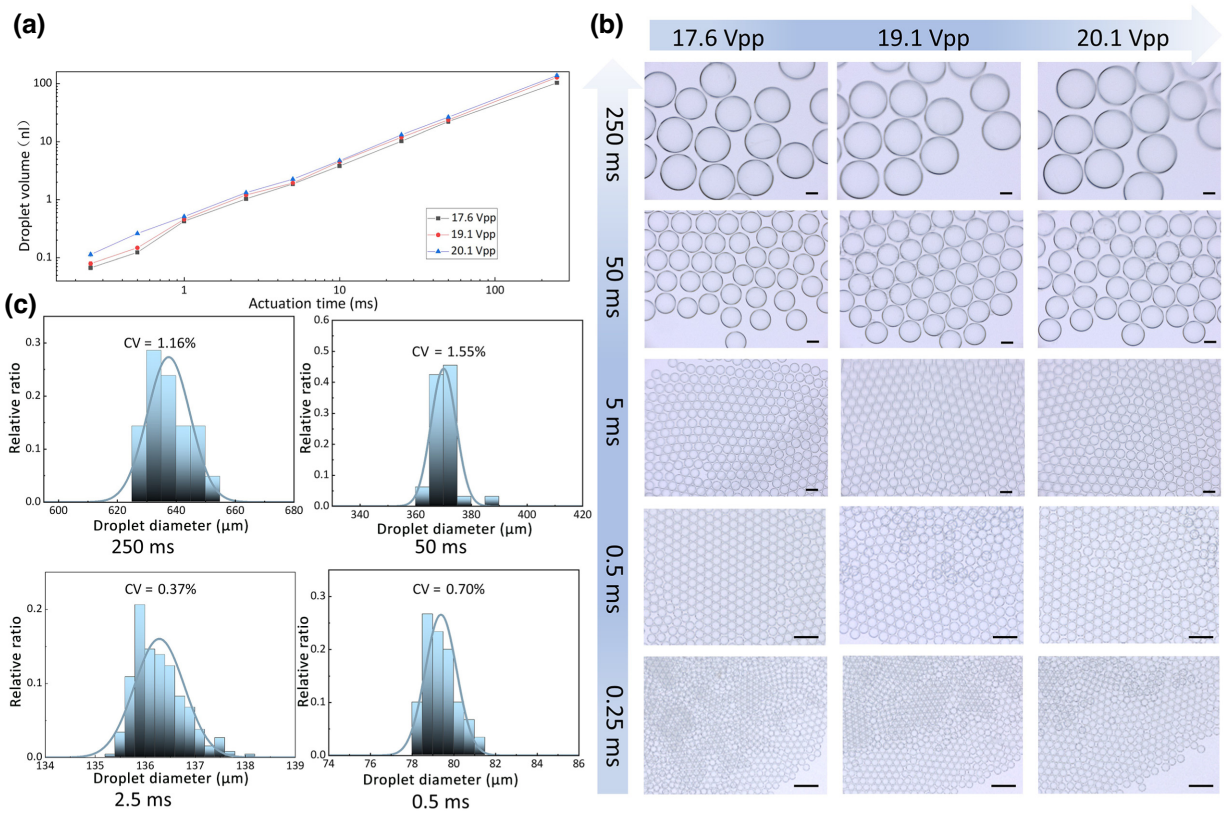

FIG. 4. Results of microdroplet generation. (a) The relationship between droplet volume and actuation time under different input voltages of 17.6 Vpp (black), 19.1 Vpp (red), 20.1 Vpp (blue), respectively. (b) Optical images show that the droplet diameters range from 641 to 50 μm at the different conditions of the actuation time and input voltages. Scale bar: 200 μm. (c) Size distribution of generated droplets at various actuation time under the input voltage of 20.1 Vpp. The coefficients of variance are all below 2%.

interfaces (defined as H). As shown in Fig. 2(b), when the H was larger than 5 cm, the water would come out from the capillary, and the flow rate increased as H increased. And the velocity reached 3.13 μl/min when the H was 7 cm. On the other hand, when the H was smaller than −3 cm (negative symbol indicates that the water-air interface was lower than oil-air interface), the oil entered the capillary, and the flow rate was 0.72 μl/min when H was set as −5 cm. Indeed, we also studied the process of the flow through the time-lapse photos. From Fig. 2(c) when H was 5 cm the water came out from the capillary, and when the gravity exceeds the capillary force the water would fall in the form of water droplets. And as shown in Fig. 2(d), when H was −3 cm, the oil entered the capillary. As above, the optimized H was between −2 and 4 cm, because the liquid level was stable in this interval [Fig. 2(e)].

After locating the position of water-oil interface at the nozzle tip, we studied the process of acoustic activated droplet generation. A FEM simulation shows that there is vibration along the axial orientation of the capillary while external acoustic source is applied [Fig. 3(b)]. Then internal fluid was subjected to the centrifugal force generated by the oscillating motion of the capillary tip, and thus was pumped out of the tip. Moreover, the vibrating capillary led to acoustic streaming in the oil phase [Fig. 3(c)], which extruded the water phase out of the nozzle tip. We experimentally verified the principle of the droplet generation process. As shown in Fig. 3(d), the process includes two parts: pumping and pinch off. When the acoustic was on, the water can be constantly pumped out from the capillary. Under high-speed microscopy, the shape of the droplet driven by vibrating nozzle tip was captured. The acoustic streaming flow dragged the extruded water phase to a spheroid with a thin connection to the nozzle tip [Fig. 3(d)], of which the thickness gradually decreases as close to the tip of the nozzle tip. When the acoustic was off, the thin connection broke up due to Laplace pressure and formed a discrete microdroplet.

As shown in Figs. 3(e) and 3(f), when the modulated acoustic wave was applied on the nozzle, discrete monodisperse microdroplets were generated. In Fig. 3(e), we set the actuation time as 5 ms. The water at the nozzle tip was pumped out from the capillary from 0 to 5 ms. At 5 ms, the acoustic signal was turned off, and then the pinch off occurred immediately, resulting in droplet generation. From 5 to 10 ms, the acoustic signal was off,

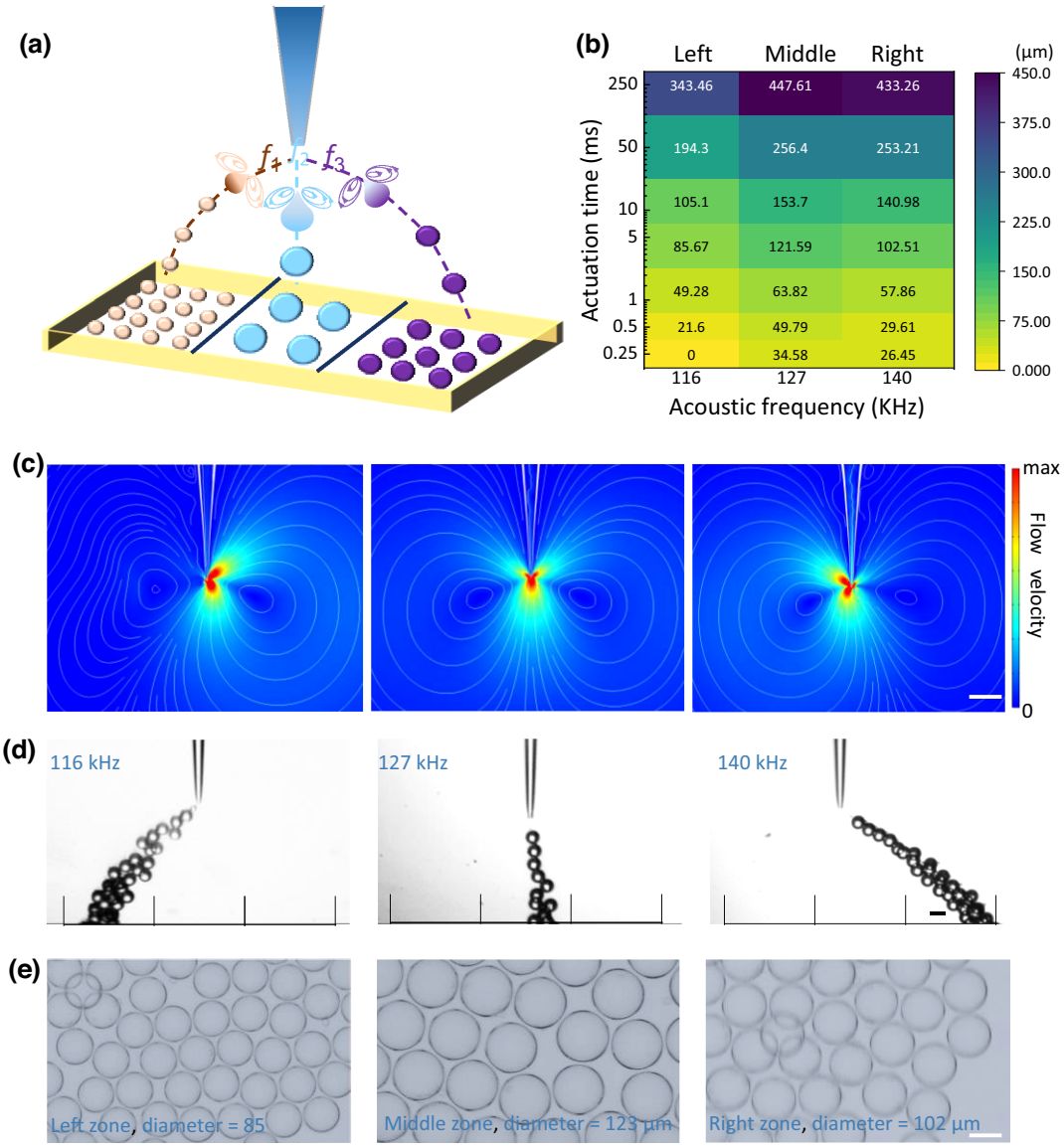

FIG. 5. Acoustic controlled microdroplet dispensing. (a) The microdroplet can be dispensed at different directions while the acoustic frequency changes. (b) Droplet size and direction in relation to acoustic frequency and actuation time. (c) Numerical simulation of the different acoustic streaming profiles with varied acoustic frequency and maximum velocity magnitude (left: 115 kHz, max: 80 um s^{-1}, middle: 125 kHz, max: 700 um s^{-1}, right: 134 kHz, max: 250 um s^{-1}). Scale bar: 200 μm. (d),(e) Combining the controls of both droplet size and directions, the droplets with on-demand sizes can be dispensed to the required collection zones, respectively. Scale bar: 100 μm.

thus the acoustic streaming stopped and there was no water extruding from the nozzle tip. This process repeated and continuously generated monodisperse microdroplets. When the actuation time decreased to 0.5 ms, a similar series of process was recorded [Fig. 3(f)], but with a smaller droplet size due to decreased water amount at each actuation period. When the actuation time was at 500 ms, the droplets fell due to gravity before the acoustic actuating ended; when the actuation time was short as 0.2 ms, it did not generate droplets. Thus, we chose the range of 0.25–250 ms for this study, at which it can produce droplets stably. This correspondence between droplet size and the acoustic actuation time allows size control of the microdroplet generation.

Besides acoustic actuation time, the droplet size might also be determined by the acoustic amplitude. We chose a voltage ranging from 17.6 to 20.1 Vpp, because it can produce droplets in a stable way across a wide range of actuation times. When the voltage was below this range, the vibration induced centrifugal force was not able to induce droplet generation, while we ran the short actuation time (0.25 ms). When the voltage was above this range, the high

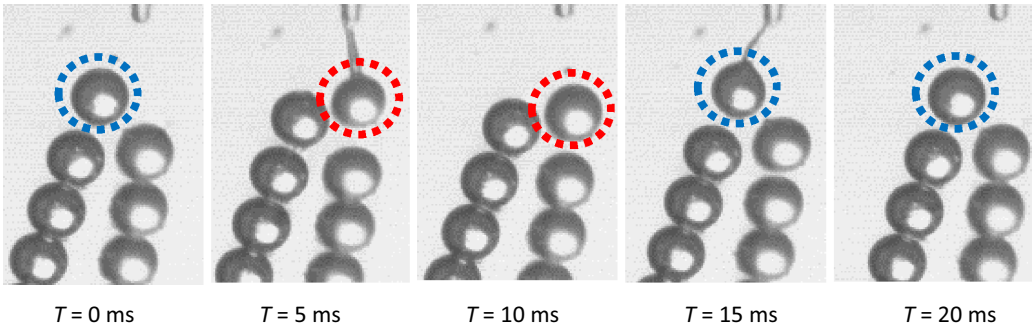

FIG. 6. Alternant same-size droplet generation and dispensing based on the acoustic actuation of controlled frequencies and amplitudes. (Left, blue; middle, red.)

pumping pressure will cause the jetting mode leading to nonuniform droplets. The increase of vibration amplitude leads to a larger centrifugal force for forming the droplet. It also increases the acoustic streaming intensity, which pumps out more fluid from the nozzle. Thus, the increase of amplitude results in larger droplets under the same actuation time. As shown in Fig. 4(a) and Table S5 within the Supplemental Material [52], we studied the relationships between droplet volume and actuation time under different input voltage. At an input voltage of 20.1 Vpp, when the actuation time was tuned from 250 ms (two droplets per second) to 0.25 ms (2000 droplets per second), the droplet volume changed from 138 ± 4.8 to 113 ± 8 pL. Besides, when the actuation time was fixed at 250 ms, the droplet volume changed from 103 to 138 nL if the voltage changed from 17.6 to 20.1 Vpp. In addition, we found a linear relationship between the volume and droplet generation rate as verified within the Supplemental Material [52]. Besides, for fluids with different alginate concentrations of 0.5, 1, and 1.5%, the corresponding dynamic viscosity is 6.09, 12.71, 24.59 mPa.s. We can also find that the linear relationship between the volume and rate of droplet generation as shown in Fig. S1 within the Supplemental Material [52]. The bigger viscosity of the liquid results in smaller droplets under the same actuation time. Moreover, we find that the culture fluid (DMEM, low glucose) can also control the generation of droplets, as shown in Fig. S3 within the Supplemental Material [52]. Correspondingly, Fig. 4(b) presented the optical images of droplets formed as a function of varying voltages and actuation time. When the actuation time was fixed, higher input voltage produced larger droplets; on the other hand, when the input voltage was fixed, longer actuation time generated smaller droplets. By modulating these two parameters, droplet diameter could be tuned from a maximum value of 641 μm (20.1 Vpp, 250 ms) to less than 50 μm (17.6 Vpp, 0.25 ms). The droplet volume accordingly ranged from 67 pL to 138 nL. The coefficient of variations (CVs) of the droplet diameters that produced under all conditions were less than 2% [Fig. 4(c)], reflecting outstanding droplet monodispersity.

In addition to the generation of droplets, the acoustic streaming flow can also be exploited to direct the droplets into different positions in a controlled manner. As shown in Fig. 5(a), a multiwell reservoir was placed in the continuous phase, the direction of droplet can be changed from left to right by changing the input acoustic frequency. With different acoustic frequency, the vibration mode of the nozzle differs, inducing the corresponding acoustic streaming flow profiles. Based on this mechanism, we can control the directions of the droplets dispensing by tuning the acoustic frequency. As shown in Fig. 5(b), while the acoustic frequency was, respectively, set as 116, 127, and 140 kHz, the microdroplets were correspondingly directed to left, middle, and right of the nozzle tip. These frequencies were selected by experimental tests across a frequency sweeping from 75 to 179 kHz with a step of 1 kHz. Moreover, the correlations between the droplet size and the actuation time stay positive along with different acoustic frequencies [Fig. 5(b)]. Numerical simulations revealed the acoustic streaming profiles and vibration modes at different acoustic frequencies [Figs. 5(c) and S4 within the Supplemental Material [52]]. Though the acoustic frequencies at the simulations (115, 125, 134 kHz) slightly differs from the experimental frequencies due to the parametric errors, the simulated acoustic streaming profiles accord well with the microdroplet dispensing directions shown in Fig. 5(d). Based on the two control mechanism: actuation time-controlled droplet size and acoustic frequency-controlled dispensing direction, we realized an integrated acoustic nozzle that can programmatically control the size and the dispensing of the microdroplets. As a demonstration, we generated 85-, 123-, and 102-μm droplets and directed them, respectively, to the left, middle, and right of the nozzle tip [Fig. 5(e)]. Besides, the acoustic streaming profiles can be changed with varied acoustic frequency under the different viscosity (0.5% alginate) of the liquid as shown in Fig. S2 within the Supplemental Material [52].

Moreover, based on the mechanism of acoustic frequency-based droplet direction, we demonstrated alternant microdroplet dispensing to the left and middle direction of the nozzle tip, as shown in Fig. 6. The pulsed

acoustic signals of 115.5 and 128.5 kHz were alternately applied to the transducer. The pulse widths kept constant at 5 ms, while the amplitudes were, respectively, 22 and 13.2 Vpp. In such a condition, the droplets were dispensed in separate directions but with the same size. The capability of simultaneous generating and dispensing the microdroplets makes it a potential tool for on-demand droplet dispensing [29,36,48].

IV. CONCLUSION

In this work, we developed an acoustic actuated microfluidic nozzle that integrates generating and dispensing of microdroplets. It is cost effective and portable, which consists of an acoustic source and a glass nozzle. Taking advantage of the huge centrifugal force generated by the vibration of the glass capillary and the optimized hydraulic pressure, it can pump liquid with a precise acoustic switch. After input a pulse modulation sinusoidal signal, uniform droplet of the required controllable size can be obtained by actively controlling the input voltage and actuation time with high throughput (2000 droplets per second), wide-range sizes (50–641 μm), and excellent monodispersity (CV under 2%). Furthermore, the system shows the capability of on-demand microdroplet dispensing. By controlling the acoustic frequency and actuation time of system, droplets of different sizes can be deposited in different reservoirs. Overall, we report an innovative simple setup for generating and dispensing microdroplets. The simplicity and the low cost of the system has potential for miniaturization and integration of droplet manipulation system, which will facilitate a variety of applications of monodisperse microdroplets.

ACKNOWLEDGMENTS

The work is supported by National Natural Science Foundation of China (Grant No. 12032015), the Innovation Program of Shanghai Municipal Education Commission (Grant No. 2019-01-07-00-02-E00030), Shanghai Pilot Program for Basic Research - Shanghai Jiao Tong University (Grant No. 21TQ1400203).

The authors declare that they have no competing interests.

[1] S.-Y. Teh, R. Lin, L.-H. Hung, and A. P. Lee, Droplet microfluidics, Lab Chip **8**, 198 (2008).
[2] O. A. Basaran, Small-scale free surface flows with breakup: Drop formation and emerging applications, Am. Inst. Chem. Eng. **48**, 1842 (2002).
[3] L. Shang, Y. Cheng, and Y. Zhao, Emerging droplet microfluidics, Chem. Rev. **117**, 7964 (2017).
[4] L. Cao, X. Cui, J. Hu, Z. Li, J. R. Choi, Q. Yang, M. Lin, L. Ying Hui, and F. Xu, Advances in digital polymerase chain reaction (dPCR) and its emerging biomedical applications, Biosens. Bioelectron. **90**, 459 (2017).
[5] H. Yuan, Y. Chao, and H. C. Shum, Droplet and Microchamber-Based Digital Loop-Mediated Isothermal Amplification (dLAMP), Small **16**, e1904469 (2020).
[6] L. Mazutis, J. Gilbert, W. L. Ung, D. A. Weitz, A. D. Griffiths, and J. A. Heyman, Single-cell analysis and sorting using droplet-based microfluidics, Nat. Protoc. **8**, 870 (2013).
[7] T. S. Kaminski and P. Garstecki, Controlled droplet microfluidic systems for multistep chemical and biological assays, Chem. Soc. Rev. **46**, 6210 (2017).
[8] H. Gudapati, M. Dey, and I. Ozbolat, A comprehensive review on droplet-based bioprinting: Past, present and future, Biomaterials **102**, 20 (2016).
[9] D. Anggraini, N. Ota, Y. Shen, T. Tang, Y. Tanaka, Y. Hosokawa, M. Li, and Y. Yalikun, Recent advances in microfluidic devices for single-cell cultivation: methods and applications, Lab Chip **22**, 1438 (2022).
[10] Y. Zheng, Z. Wu, L. Lin, X. Zheng, Y. Hou, and J.-M. Lin, Microfluidic droplet-based functional materials for cell manipulation, Lab Chip **21**, 4311 (2021).
[11] W. Feng, L. Li, X. Du, A. Welle, and P. A. Levkin, Single-step fabrication of high-density microdroplet arrays of low-surface-tension liquids, Adv. Mater. **28**, 3202 (2016).
[12] P. Zhu and L. Wang, Passive and active droplet generation with microfluidics: a review, Lab Chip **17**, 34 (2016).
[13] Y. Zhu, Y. X. Zhang, L. F. Cai, and Q. Fang, Sequential operation droplet array: an automated microfluidic platform for picoliter-scale liquid handling, analysis, and screening, Anal. Chem. **85**, 6723 (2013).
[14] X. L. Guo, Y. Wei, Q. Lou, Y. Zhu, and Q. Fang, Manipulating femtoliter to picoliter droplets by pins for single cell analysis and quantitative biological assay, Anal. Chem. **90**, 5810 (2018).
[15] T. Thorsen, R. W. Roberts, F. H. Arnold, and S. R. Quake, Dynamic Pattern Formation in a Vesicle-Generating Microfluidic Device, Phys. Rev. Lett. **86**, 4163 (2001).
[16] P. Garstecki, M. J. Fuerstman, H. A. Stone, and G. M. Whitesides, Formation of droplets and bubbles in a microfluidic T-junction-scaling and mechanism of break-up, Lab Chip **6**, 437 (2006).
[17] P. Garstecki, I. Gitlin, W. DiLuzio, G. M. Whitesides, E. Kumacheva, and H. A. Stone, Formation of monodisperse bubbles in a microfluidic flow-focusing device, Appl. Phys. Lett. **85**, 2649 (2004).
[18] H. Kim, D. Luo, D. Link, D. A. Weitz, M. Marquez, and Z. Cheng, Controlled production of emulsion drops using an electric field in a flow-focusing microfluidic device, Appl. Phys. Lett. **91**, e133106 (2007).
[19] C. Cramer, P. Fischer, and E. J. Windhab, Drop formation in a co-flowing ambient fluid, Chem. Eng. Sci. **59**, 3045 (2004).
[20] D. R. Link, E. Grasland-Mongrain, A. Duri, F. Sarrazin, Z. Cheng, G. Cristobal, M. Marquez, and D. A. Weitz, Electric control of droplets in microfluidic devices, Angew. Chem., Int. Ed. Engl. **45**, 2556 (2006).

[21] N.-T. Nguyen, Micro-magnetofluidics: Interactions between magnetism and fluid flow on the microscale, Microfluid. Nanofluid. **12**, 1 (2012).
[22] C. N. Baroud, M. R. de Saint Vincent, and J. P. Delville, An optical toolbox for total control of droplet microfluidics, Lab Chip **7**, 1029 (2007).
[23] N.-T. Nguyen, T.-H. Ting, Y.-F. Yap, T.-N. Wong, J. C.-K. Chai, W.-L. Ong, J. Zhou, S.-H. Tan, and L. Yobas, Thermally mediated droplet formation in microchannels, Appl. Phys. Lett. **91**, e084102 (2007).
[24] K. T. Kroll, Daniele Foresti, Robert Amissah, Francesco Sillani, Kimberly A. Homan, Dimos Poulikakos, and Jennifer A. Lewis, Acoustophoretic printing, Sci. Adv. **4**, e1659 (2018).
[25] Z. Z. Chong, S. H. Tan, A. M. Ganan-Calvo, S. B. Tor, N. H. Loh, and N. T. Nguyen, Active droplet generation in microfluidics, Lab Chip **16**, 35 (2016).
[26] J. Guerrero, Y. W. Chang, A. A. Fragkopoulos, and A. Fernandez-Nieves, Capillary-based microfluidics-coflow, flow-focusing, electro-coflow, drops, jets, and instabilities, Small **16**, e1904344 (2020).
[27] H. Tian, Y. Sun, C. Liu, X. Duan, W. Tang, and Z. Li, Precise quantitation of microRNA in a single cell with droplet digital PCR based on ligation reaction, Anal. Chem. **88**, 11384 (2016).
[28] X. Li, D. Zhang, W. Ruan, W. Liu, K. Yin, T. Tian, Y. Bi, Q. Ruan, Y. Zhao, Z. Zhu, *et al.*, Centrifugal-driven droplet generation method with minimal waste for single-cell whole genome amplification, Anal. Chem. **91**, 13611 (2019).
[29] Y. Qin, L. Wu, J. Wang, R. Han, J. Shen, J. Wang, S. Xu, A. L. Paguirigan, J. L. Smith, J. P. Radich, *et al.*, A fluorescence-activated single-droplet dispenser for high accuracy single-droplet and single-cell sorting and dispensing, Anal. Chem. **91**, 6815 (2019).
[30] J. C. Baret, O. J. Miller, V. Taly, M. Ryckelynck, A. El-Harrak, L. Frenz, C. Rick, M. L. Samuels, J. B. Hutchison, J. J. Agresti, *et al.*, Fluorescence-activated droplet sorting (FADS): efficient microfluidic cell sorting based on enzymatic activity, Lab Chip **9**, 1850 (2009).
[31] D. Sun, K. F. Bohringer, M. Sorensen, E. Nilsson, J. S. Edgar, and D. R. Goodlett, Droplet delivery and nebulization system using surface acoustic wave for mass spectrometry, Lab Chip **20**, 3269 (2020).
[32] H. D. Xi, H. Zheng, W. Guo, A. M. Ganan-Calvo, Y. Ai, C. W. Tsao, J. Zhou, W. Li, Y. Huang, N. T. Nguyen, *et al.*, Active droplet sorting in microfluidics: A review, Lab Chip **17**, 751 (2017).
[33] Y. Yuan, J. Brouchon, J. M. Calvo-Calle, J. Xia, L. Sun, X. Zhang, K. L. Clayton, F. Ye, D. A. Weitz, and J. A. Heyman, Droplet encapsulation improves accuracy of immune cell cytokine capture assays, Lab Chip **20**, 1513 (2020).
[34] Thomas Franke, David A. Weitza, and Achim Wixforthb, Surface acoustic wave (SAW) directed droplet flow in microfluidics for PDMS devices, Lab Chip **9**, 2625 (2009).
[35] L. Schmid, D. A. Weitz, and T. Franke, Sorting drops and cells with acoustics: acoustic microfluidic fluorescence-activated cell sorter, Lab Chip **14**, 3710 (2014).
[36] F. Huang, Z. Zhu, Y. Niu, Y. Zhao, T. Si, and R. X. Xu, Coaxial oblique interface shearing: tunable generation and sorting of double emulsions for spatial gradient drug release, Lab Chip **20**, 1249 (2020).
[37] Z. Wang and J. Zhe, Recent advances in particle and droplet manipulation for lab-on-a-chip devices based on surface acoustic waves, Lab Chip **11**, 1280 (2011).
[38] T. Wriedt, Norbert Riefler and Udo Fritsching Impedance characterization of a coupled piezo-tube-fluid system for micro droplet generation, J. Fluids Struct. **88**, 185 (2019).
[39] J. R. F. Ming, K. Tan, and Leslie Y. Yeo, Interfacial Jetting Phenomena Induced by Focused Surface Vibrations, Phys. Rev. Lett. **103**, 024501 (2009).
[40] U. Demirci and G. Montesano, Single cell epitaxy by acoustic picolitre droplets, Lab Chip **7**, 1139 (2007).
[41] M. He, Y. Zhou, W. Cui, Y. Yang, H. Zhang, X. Chen, W. Pang, and X. Duan, An on-demand femtoliter droplet dispensing system based on a gigahertz acoustic resonator, Lab Chip **18**, 2540 (2018).
[42] Z. He, J. Wang, B. J. Fike, X. Li, C. Li, B. L. Mendis, and P. Li, A portable droplet generation system for ultra-wide dynamic range digital PCR based on a vibrating sharp-tip capillary, Biosens. Bioelectron. **191**, 113458 (2021).
[43] C. Ding, Y. Liu, Y. Guo, X. Guo, Q. Kang, X. Yan, and Z. He, Precise digital bacteria enumeration and antibiotic susceptibility testing via a portable vibrating capillary-based droplet platform, Sens. Actuators, B **380**, 133254 (2023).
[44] J. C. Brenker, D. J. Collins, H. Van Phan, T. Alan, and A. Neild, On-chip droplet production regimes using surface acoustic waves, Lab Chip **16**, 1675 (2016).
[45] M. Sesen, T. Alan, and A. Neild, Microfluidic on-demand droplet merging using surface acoustic waves, Lab Chip **14**, 3325 (2014).
[46] I. Leibacher, P. Reichert, and J. Dual, Microfluidic droplet handling by bulk acoustic wave (BAW) acoustophoresis, Lab Chip **15**, 2896 (2015).
[47] P. Li, Z. Ma, Y. Zhou, D. J. Collins, Z. Wang, and Y. Ai, Detachable acoustophoretic system for fluorescence-activated sorting at the single-droplet level, Anal. Chem. **91**, 9970 (2019).
[48] Y. Zhu, X. Zhang, L. Sun, Y. Wang, and Y. Zhao, Engineering human brain assembloids by microfluidics, Adv. Mater., e2210083 (2023).
[49] B. Huang, Dege Li, Yi Cao, Molong Han, Xinlei Wu, Qiang Sun, Chi Ma, Lilong Zhao, Peng Liu, Chao Zheng, Hang Dong, Xiaolong Wang, Yonghong Liu, and Yanzhen Zhang, Confined interface vibration for femtoliter droplets generation and manipulation, Nano Select **2**, 338 (2021).
[50] Rune Barnkob, Peter Barkholt Muller, Mads Jakob Herring Jensen, and Henrik Bruus, A numerical study of microparticle acoustophoresis driven by acoustic radiation forces and streaming-induced drag forces, Lab Chip **12**, 4617 (2012).
[51] Q. Tang and J. Hu, Diversity of acoustic streaming in a rectangular acoustofluidic field, Ultrasonics **58**, 27 (2015).
[52] See Supplemental Material at http://link.aps.org/supplemental/10.1103/PhysRevApplied.20.024067 for descriptions of the numerical simulation and relationship between the volume and frequency of droplets, Figs. S1–S4, and Tables S1–S5.